The Structural Characteristics of Carbon Nanoparticles Produced by Arc Discharge in Toluene Without Added Catalyst or Gases

Isya Fitri Andhika
Master of Chemistry Program, Graduate School, Sebelas Maret University

Teguh Endah Saraswati
Department of Chemistry, Faculty of Mathematics and Natural Sciences, Sebelas Maret University

Hastuti, Sri
Department of Chemistry, Faculty of Mathematics and Natural Sciences, Sebelas Maret University

https://doi.org/10.5109/4068622

出版情報：Evergreen. 7 (3), pp.417-428, 2020-09. 九州大学グリーンテクノロジー研究教育センター
バージョン：

The Structural Characteristics of Carbon Nanoparticles Produced by Arc Discharge in Toluene Without Added Catalyst or Gases

Isya Fitri Andhika[1], Teguh Endah Saraswati[2*], and Sri Hastuti[2]

[1]Master Program of Chemistry, Faculty of Mathematics and Natural Sciences, Sebelas Maret University, Jl. Ir. Sutami 36 A Surakarta 57126 Indonesia

[2]Department of Chemistry, Sebelas Maret University, Jl. Ir. Sutami 36 A Surakarta 57126 Indonesia

* Author to whom correspondence should be addressed:
E-mail: teguh@mipa.uns.ac.id

(Received January 15, 2020; Revised June 6, 2020; accepted September 3, 2020).

Abstract: Carbon nanoparticles (CNPs) have been intensively explored due to their wide applications. One of the cost-effective synthesis techniques is arc discharge in liquid, which produces various carbon nanostructures depending on environmental conditions such as catalyst and gases. The use of organic compound, e.g., toluene, acts as a carbon source for carbon nanoparticle growth. However, the carbon structure examinations of the CNPs product deposited in different spots produced by arc discharge in toluene without added catalyst and gases have not been studied in detail. Therefore, the present study investigates the structural characteristics of CNPs produced by arc discharge in pure toluene using Fourier transform infrared (FTIR), X-ray diffraction (XRD), scanning electron microscopy equipped by electron dispersive spectroscopy (SEM-EDS) transmission electron microscope (TEM) imaging data. The nanoparticles were collected by scraping powder from four different spots: the electrode handles; the space between the electrodes; in the liquid medium; and at the bottom of the reaction chamber. The C(002) peak analyzed in the diffraction pattern of CNPs collected in these locations shows different intensities and features. The CNPs formed between the electrodes had the most crystalline graphitic structures. The Fourier transform infrared (FTIR) spectra show differences in the C−H absorption, especially for CNPs dissolved in toluene, suggested contains fullerene and its organic hydrocarbon fragments. Moreover, a Raman analysis shows significant differences between the CNPs deposited between the electrodes and those collected from the bottom of the glass chamber, which validates the FTIR, XRD, and TEM imaging data. The powder deposited between the electrodes seems to take the form of CNPs with better graphitic structures; meanwhile, powder collected from the other spots were analyzed to be hydrogenated diamond-like carbon and glassy bulk carbon.

Keywords: arc discharge, carbon, nanoparticles, toluene, structural characteristics

1. Introduction

Carbon nanoparticles (CNPs) are zero dimensional-carbon allotropes which have attracted extensive research interest due to their wide applications such as in potential applications in materials science[1)], energy[2)], photovoltaic science[3)], nanodevices[4)], biosensor[5)], and biomedicine[6)]. The carbon allotropes have a crystalline phase with bonds consisting of sp^2 or sp^3 carbon, oxygen- or nitrogen-based groups, and post-modified chemical groups[7)]. The synthesis of CNPs has been developed in various methods such as microwaves[8)], thermal decomposition[9)], ultrasonic synthesis[10)], or chemical vapor deposition[11)], electrochemical methods[12)], laser ablation[13)], coaxial arc plasma deposition (CAPD)[14)], and arc discharge[15)].

One of the other forms of a nanocrystalline phase of carbon is called glassy carbon or glass-like carbon (GC) produced by pyrolysis of organic polymer. GC is classified in non-graphitizing carbon; however, it is not an amorphous carbon. GC has a turbostratic type structure composed of micro or nanocrystalline graphite-like layers arranged in ribbons with disordered regions[16, 17)]. One of the applications of glassy carbon is for coating the biomedical tools.

The non-crystalline carbons known as amorphous carbon are a mixture consisting of sp^3, sp^2, and sp^1 hybridized carbon atoms. A high fraction of sp^3 bonds exists in diamond-like carbon (DLC). The properties are

depending on sp^3/sp^2-hybridized carbon and hydrogen or nitrogen content[18]. DLC is also generally applied as coating layers improving the metal corrosion or wear resistance. This kind of material can be grown by several deposition techniques such as cathodic vacuum arc, pulsed laser deposition[18], electrodeposition[19], direct current plasma jet, and microwave chemical vapor deposition[20], and electrolysis[21].

The arc discharge has several advantages, including a technically simple experimental setup that can produce self-crystallized nanostructures thanks to its high-temperature processes, low impurity levels, low cost, and a high yield of nanoparticles[22]. In this tecnique, an arc is generated between two graphitic rods kept at a distance of a few millimeters[23].

In submerged arc discharge, which was introduced by Sano et al., graphite electrodes are placed in a liquid medium of water in order to produce carbon anions[24]. Research into submerged arc discharge in liquid medium has been conducted using metal or metal-filled graphite electrodes to produce carbon nanotubes (CNTs)[25-27].

The type of medium used in submerged arc discharge is one of the parameters that determine which kinds of CNPs will be produced. Liquid nitrogen provides an oxygen-free environment for reaction[28]. De-ionized water has good cooling capabilities and lower evaporation levels than liquid nitrogen, and it can insulate the reaction from atmospheric oxygen[23]. Submerged arc discharge in water produces oxygen-containing gas, which is possibly involved in CNPs growth, inducing the destruction of the graphitic layers forming oxygenated amorphous carbon[29].

Muthakarn et al. used alcohols, alkanes, and aromatics as a medium of the submerged arc with continuous purge with N_2[29], resulting in various structures of CNPs. The use of this gas is intended to prevent explosions during arc discharge. Beck et al. used other submerged arc discharge medium of aromatic hydrocarbon, which is toluene ($C_6H_5CH_3$), without gases. The results were confirmed by gas chromatography-mass spectrometer (GC-MS) as fullerene and polycyclic aromatic hydrocarbon; however, a further physical and structural characterization of the products was not provided[30]. Okada et al. used toluene as arc discharge medium with graphite and Mo, Fe, Ni as electrodes for producing carbon nanotubes[26]. The use of catalysts, even though it has been proven able to enhance the graphitic layers, the catalyst removal steps should be performed after the synthesis process to obtain the purified products. In general, the purification steps need to be conducted in several steps of chemical oxidation, physical separation, and combinations of chemical and physical techniques using acids and organic solvents[31], which made this technique inconvenience.

The arc discharge technique in the liquid medium of pure toluene is a simpler method compared to the same using additional catalyst or gases. However, to date, there have been no studies that attempted to do the same without the use of gas. The structure of CNPs at their location of formation has not been studied in detail, neither in cases of submerged arc discharge or conventional arc discharge.

To this end, this study investigates the structure of carbon materials obtained from a simple synthesis by the submerged arc discharge method in a toluene medium, using graphite electrodes, without the addition of metal catalysts or the use of gas. This process is expected to produce CNPs in different structures of carbon allotropes, depending on the deposited spots. The interesting findings of this study, we confirmed the CNPs structures such as hydrogenated diamond-like carbon (DLC) and glass-like carbon (GC). Synthesis without catalyst or gases was performed in purpose to avoid the defect by the substitutions of non-carbon atoms, e.g., oxygen and nitrogen, coming from catalyst or gases. To the best of our knowledge, these carbon forms have not been explored by pioneering works related to carbon arc discharge in liquid.

2. Materials and Method

The experimental arc discharge setup consisted of two electrodes from a graphite rod (anode and cathode: ϕ 10 mm; length 20 mm; Qingdao Tenry Cardon Co. Ltd; carbon 99%; density 1.95 gr/cm^3; electrical resistance 7-10 ohm) submerged in 300 mL of 99.9% toluene (Merck) in a glass beaker. The electrodes used were graphite electrodes with the tip of the blunt end forming the cathode and the tip of the tapered end forming the anode, in order to facilitate the arc discharge during the synthesis process. Toluene was used as a liquid medium in the arc discharge process as a carbon source for carbon nanoparticle formation. The graphite anode and cathode were submerged in a beaker containing toluene with a narrow gap and were connected to a direct current (DC) power supply (Krisbow, 10-100 Amps, 20-30 Volts). The discharge was stable as long as the cathode-anode gap was less than one millimeter, the current was flowing at 30 A, and the voltage at ~20 V.

One course experiment took place in a total time of approximately 1 hour, in which there were five sets of discharging. One set discharging experiment consisted of five arc events. Each arc occurred for around 20 seconds. A pause time was given between two events for 10 minutes for cooling the medium. After the arc discharge process, the CNPs soot generated by the arc discharge plasma over the course were found inside and were collected from different spots. CNPs created by the arc discharges in toluene were classified into four types, based on the location where they had formed. CNPs formed on the arc handle were referred to as CNPs-A; those formed between the electrodes were CNPs-B; those found in the toluene solution were called CNPs-C; and those precipitated in the bottom of the beaker was CNPs-

D. Each of the different CNPs was dried and heated up to 110 °C under a fume hood.

In the case of CNPs-C, which were found in the toluene, the sample was evaporated using a rotary evaporator (Eyela N-11000). To avoid the mixing of CNPs-C into CNPs-D, CNPs-D was further purified by immersion in toluene in a 1:10 (w/v) ratio. A further heating treatment was done using an annealed thermal vacuum in a horizontal tube furnace (OTF 1200X) with a quartz tube (ϕ= 75 mm; t= 1 mm) at 250 °C and heated at a rate of 5 °C/min for six hours. The purified CNPs-D was namely CNPs-D'. Further characterization was then performed.

The structural characterizations of the CNPs were analyzed using X-ray diffraction (XRD, Philips X'pert Pro; Cu 1.54 Å, generator setting 30 mA, 40 kV, diffraction angle 5.0084–79.9784^{o}), Fourier transform infrared (FTIR, Shimadzu IR Prestige-21), transmission electron microscopy (TEM, FEI Tecnai G2 20S-Twin; 200kV), scanning electron microscopy equipped by electron dispersive spectroscopy (SEM-EDS, Merk FEI, Type: Inspect-S50), Raman spectroscopy (Horiba Scientific, Modular Raman type iHR 320; laser 532 nm). The further quantitative study of the crystallite size (D) of each CNPs was estimated using the XRD pattern. The size of the crystal was determined by Scherer's method[32], using equation (1). Crystallite size (D) is calculated by a constant value (k) of 0.9, multiplied by the X-ray wavelength (λ), and divided by the multiplication result of the B value with cos θ. B is FWHM (full width at half maximum) in radians, (Bragg's angle), while the value of θ can be known from 2θ of the associated peaks.

$$D = \frac{k\,\lambda}{B\cos\theta} \qquad \ldots\ldots\ldots (1)$$

3. Results and Discussion

As the process of submerged arc discharge in toluene began, the initially clear toluene solution became black, as shown in Figure 1. The arc occurred between anode and cathode and was only stable when the electrode gap was less than one millimeter. An arc reaction took place in a short duration. The arc process creates a spark between the two electrodes submerged in toluene. After the arc discharge process, the deposited soot generated was collected from different spots of A through D (see Figure 1).

CNPs-A and -B were collected from the handle of the electrodes and between the electrodes, respectively. CNPs-C was collected from the liquid medium of toluene. The resulting all separated CNPs are described as solid black powders of certain masses, as listed in Table 1. The results showed that the highest yield of CNPs was formed between electrodes (CNPs-B). After the arc discharging process, no reduction in mass in the anode and cathode, indicating that the CNPs deposits were highly possible formed from the carbon source of the liquid medium of toluene. In addition, no reduction/corrosion on carbon electrodes make them reusable in subsequent submerged arc discharge processes.

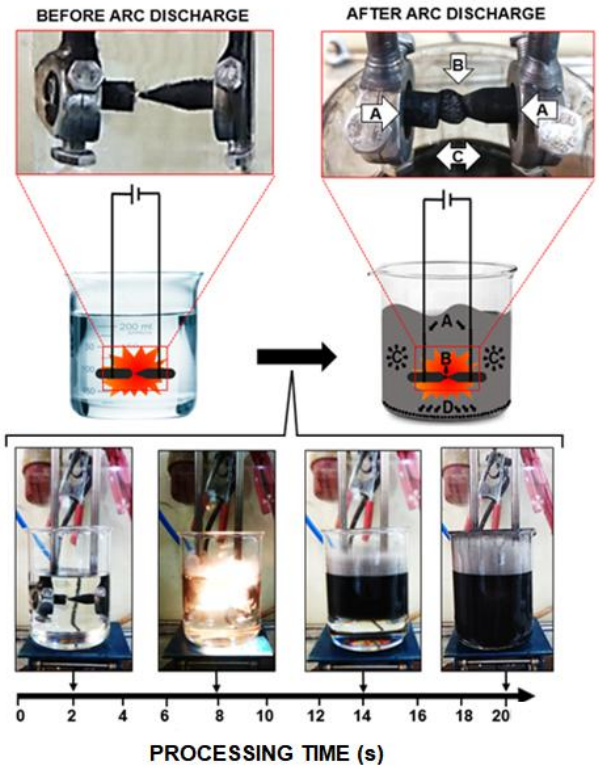

Fig 1: The process of CNP synthesis by arc discharge in toluene. A through D are CNPs collected from the handle of the electrodes, between the electrodes, from the liquid toluene medium, and from the bottom of the beaker glass, respectively.

Table 1. Mass of CNPs synthesized by arc discharge in toluene.

Carbon nanoparticles (CNPs)	Mass (g/one experiment)*
A	0.0188 ± 0.001
B	0.6382 ± 0.002
C	0.1523 ± 0.003
D	0.1011 ± 0.003

*Conditions: rod length, 20 mm; diameter, 10 mm; liquid medium, 300 mL toluene; DC 30 A (~20 V); one set experiment was defined in the method.

CNPs were further characterized in order to study structural characteristics based on the location where they were formed. The process of submerged arc discharge in toluene using graphite electrodes supposedly produces nanoparticle structures of various carbon allotropes in different locations. When an arc occurred, the hot plasma zone occurs between the anode and the cathode, vaporizing and ionizing the carbon compounds decomposed from the toluene. Carbon vapors then condensed into CNPs and deposited in the different spots, which initially form on the electrode surface and are dispersed in the liquid medium, then fall

to the bottom of the beaker glass (CNPs-D). The identification of the functional groups attached to the CNPs was conducted using FTIR spectra.

Figure 2 shows the FTIR spectra of CNPs-A through -D and the purified CNPs-D as CNPs-D'. The FTIR spectra of CNPs-A through -D' (except CNPs-B) show a functional group such as C=C stretching from aromatic ring (1500-1600 cm^{-1}). The C=C bond of the aromatic ring shows the character of the structure of the carbon allotrope from the graphite, CNT, graphene, or fullerene structure. The C=C bonding possibly connected with the other functional groups confirmed by other observable absorption peaks at the different wavenumber[33)].

The FTIR spectra of CNPs-A and C show more rich peaks as compared to the others. For example, as confirmed in the FTIR spectrum of CNPs-A, it has the absorption peak at 2921.32 cm^{-1} and 2852.84 cm^{-1}, which are corresponding to the asymmetrical and symmetrical stretching of =C−H, respectively. These characteristics are indicative of modified sp^2 hybridized C atom in C=C of the basic hexagonal carbon structure of graphite with hydrogen atoms. Therefore, from these interpreted data, CNPs-A has a highly possible structure of graphite-like carbon defected by hydrogen atoms which replaced the double bonds in the basic hexagonal aromatic carbon ring. A broad vibration O−H at a wavenumber of ~3400 cm^{-1} suggests to the molecules of H_2O vapor adsorbed on CNPs-A. Meanwhile, absorption signed by the star (*), as shown in Figure 2, represented the high wavenumber range for carbon dioxide (2250 to 2400 cm^{-1}) and low wavenumber range for carbon dioxide (600 to 740 cm^{-1})[34)].

On the other hand, the FTIR spectrum of CNPs-B shows almost no absorption peaks, which plausible for the characteristic of the symmetrical C=C in graphite structure without connected to other functional groups[33, 35)]. However, this suggestion would be further confirmed later by XRD analysis.

The FTIR spectrum of CNPs-C has a different pattern, among others. The revealed pattern shows absorptions at 2961.82 cm^{-1}, 2924.21 cm^{-1}, and 2853.81 cm^{-1}, which are corresponding to symmetrical stretching of −C−H (which possibly comes from $-CH_3$), the asymmetrical, and symmetrical stretching of =C−H, respectively[35, 36)]. As well as CNPs-A, the suggested structure of CNPs-C is highly possible as defected graphite structure by hydrogen atoms. The presenting peak of C−H bending at a wavenumber of 800.49 cm^{-1} strengthens this suggestion. Moreover, the absorption peaks appeared at a wavenumber of 1261.50 cm^{-1} and a couple of peaks of 1020.39 cm^{-1} and 1021.35 cm^{-1}, also attribute to C−C and aromatic C−H in-plane bending, respectively[36)]. These presenting peaks might attribute to C−H connected to C atoms in the hexagonal graphitic structure. These suggested structures later are intensely discussed in the discussion of XRD analysis.

The FTIR spectrum of CNPs collected from the bottom of the chamber (CNPs-D) reveals an almost identical FTIR profile to that of purified CNPs (CNPs-D'). The FTIR spectra of both CNPs-D and CNPs-D' shows nearly the same with the typical characteristics of the FTIR spectrum of graphite with fairly minimal absorption. These spectra show the absorption of functional groups O−H and C−H, respectively, as a

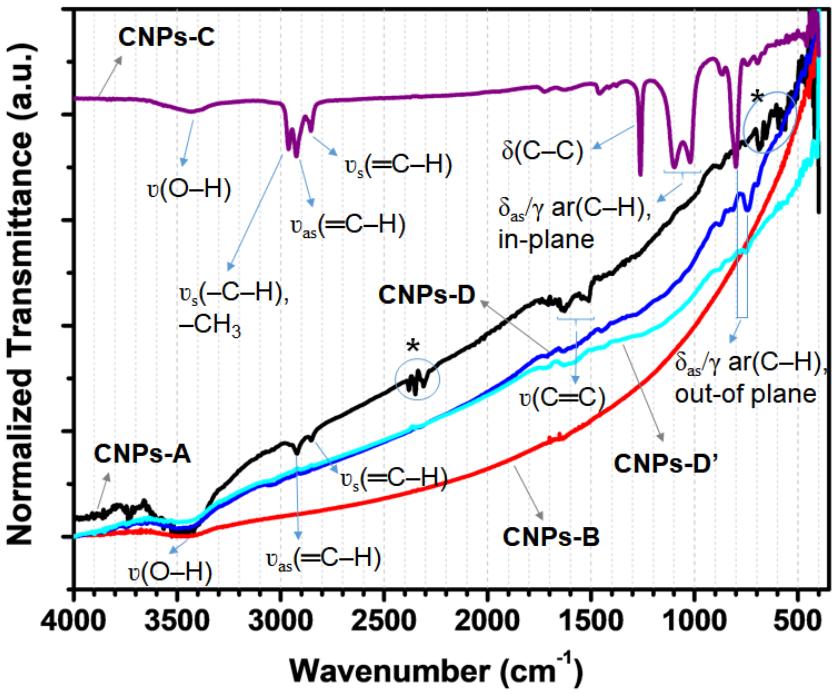

Fig 2: FTIR spectra of CNPs-A, CNPs-B, CNPs-C, and CNPs-D, and the purified CNPs-D as CNPs-D' (* is represented to CO_2).

broad and a weak peak feature in the wavenumber of ~3400 cm^{-1} and ~743 cm^{-1}. The later peak of bending C−H with weak feature suggests the few hydrogen substitutions[37]. This similar pattern becomes the reason for the subsequent analysis was then only performed for CNPs-D'.

As a premature discussion in the section of FTIR analysis, the O−H stretching at wavenumbers ~3400 cm^{-1} observable in the FTIR spectra indicates the hydroxyl group is related to the hydroxyl of physically absorbed H_2O vapor molecules, rather than from hydroxyl that is covalently linked to carbon as C−OH. Moreover, CNPs deposited between electrodes (CNPs-B) and settled in the bottom of the beaker glass (CNPs-D and -D') are possibly having a graphitic structure with a minimum defect caused by hydrogen atom substitutions. Meanwhile, CNPs-C has less dominant graphitic structure, because it was mostly composed of the condensed toluene fragments which have many hydrogen atoms, resulting in more dispersable in toluene.

In order to confirm the crystalline structures and properties of CNPs, the characterization was then continuously analyzed by X-ray diffraction (XRD), as shown in Figure 3. To further confirm the crystallinity, the crystallite sizes (*D*) of graphitic phase of CNPs were estimated, as presented in Table 2.

The diffractograms of CNPs-A, -B, and -D', revealed the presence of graphite peaks at hkl C(002), (100), (004), and (110) at 2θ = 25.83°, 42.40°, 53.62°, 77.53°, respectively, with different intensities. This feature match to diffraction spectra database of graphite hexagonal (PDF#41-1487, the database quality marks (QM): indexed (I); indexed QM means that the diffraction pattern has been indexed; thus, the material is almost certainly in a single-phase). The presence of C(002) in the diffraction pattern of CNPs-A, -B, and –D, with different features and intensities, indicates that these CNPs have a crystalline structure of graphitic carbon in different crystallinity degree, estimated from the feature peak of C(002). If the peak is in a sharp feature with higher intensity, thus the graphitic structure has better crystallinity due to the bigger crystallite size. Oppositely, if the peak of C(002) is in a broader feature, it has a lower crystallinity degree, indicative of the presence of defects on the graphitic carbon structure.

Comparing to CNPs-B, CNPs-A and D have lower intense C(002) peak, in which CNPs-A is the lowest one, indicative of the most defected structures. The defected graphitic structures of CNPs-A revealed is plausible in a turbostratic structure because the diffraction peak of C(002) is broader compared to that of graphite powder[38]. Moreover, taking a look in detail the XRD pattern of CNPs-A, it has the other two observable sharp peaks at 43.46° and 77.17°, which corresponds to the diamond crystal of D(111) and D(220), respectively. The diffraction database used to analyze these two peaks is the diffraction pattern of diamond in PDF#06-0675 (QM: star (S); star QM defined that the database was taken in a high-quality diffractometer in which the chemical composition has been well-characterized).

The presence of the diamond–corresponding peaks highly relates to the defects that occurred in the graphitic carbon of CNPs-A. A broader feature C(002) peak indicates sp^2 bonded carbon in graphitic structures evolves to sp^3 bonded carbon. Based on the FTIR spectrum of CNPs-A, this evolution is due to hydrogen atom substitutions because the FTIR spectrum of CNPs-A shows the presence of stretching vibration of C-H around 3000 − 2800 cm^{-1}. The data concludes that CNPs-A has hydrogenated DLC because it contains sp^3-bonded

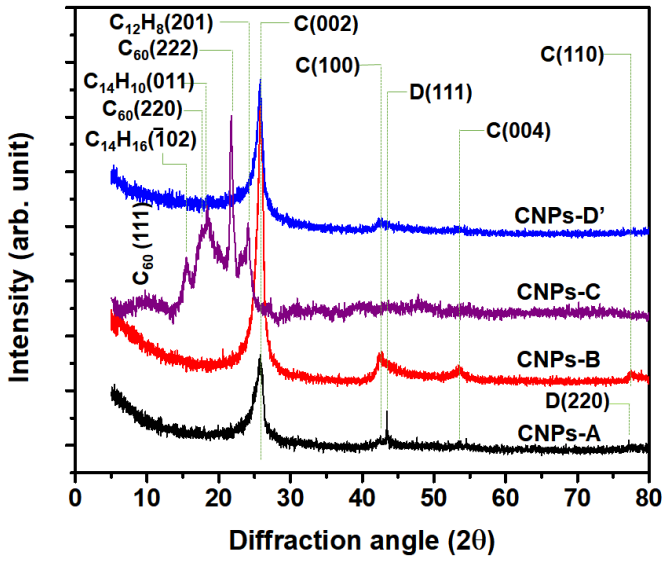

Fig 3: XRD pattern of CNPs-A, CNPs-B, CNPs-C, and CNPs-D'.

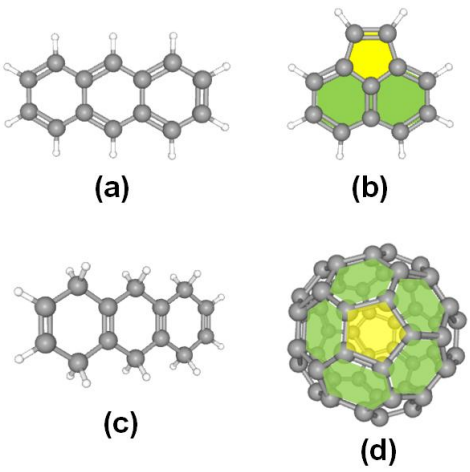

Fig 4: The molecular structure of (a) anthracene, (b) acenaphthylene, (c) 1,4,5,8,9,10-Hexahydroanthracene, and (d) fullerene C_{60}. The yellow and green shades are assigned to the pentagonal dan hexagonal carbon ring.

Table 2. The crystallite size of CNPs synthesized in toluene using arc discharge.

Identified peaks	CNPs-A			CNPs-B			CNPs-C			CNPs-D		
	2Θ (°)	B (°)	D (nm)	2Θ (°)	B (°)	D (nm)	2Θ (°)	B (°)	L (nm)	2Θ (°)	B (°)	D (nm)
$C_{14}H_{16}$ (ī02)	-	-	-	-	-	-	15.53	0.39	20.35	-	-	-
$C_{14}H_{10}$ (011)	-	-	-	-	-	-	18.42	1.77	4.55	-	-	-
C_{60} (222)	-	-	-	-	-	-	21.65	0.37	22.10	-	-	-
$C_{12}H_8$ (201)	-	-	-	-	-	-	24.13	0.28	29.54	-	-	-
C (002)	25.80	1.02	7.96	25.79	0.82	9.91	-	-	-	25.67	1.08	7.55
C(100)	-	-	-	42.34	1.14	7.47	-	-	-	43.06	2.19	3.89
D(111)	43.38	0.10	84.87	-	-	-	-	-	-	-	-	-

carbon with hydrogen atoms. In addition, the XRD data of CNPS-A is in line with the XRD pattern of diamond-like carbon (DLC) synthesized by electrodeposition[19], direct current plasma jet, microwave chemical vapor deposition[20], and electrolysis[21].

Meanwhile, CNPs-C has the most distinct diffraction patterns. CNPs-C collected in toluene highly possible is not graphite or other carbon materials with higher aspect ratio i.e., graphite, etc. which are non-dissolvable in toluene. Therefore, in the diffraction pattern of CNPs-C, no peak C(002) as a graphite characteristic was observable. However, several peaks around $2\theta < 25^{o}$ appeared represented to fullerene and its derivatives. CNPs-C revealed several peaks located 2θ 10.83°, 15.48°, 17.62°, 18.42°, 21.78°, and 24.08°, correspond to C_{60}(111), $C_{14}H_{16}$(102), C_{60}(220), $C_{14}H_{10}$(011), C_{60}(222), and $C_{12}H_8$(201), respectively. These assignments refer to the diffraction pattern database of Buckminsterfullerene C_{60} (PDF#44-0558, QM: star, S), 1,4,5,8,9,10-Hexahydroanthracene $C_{14}H_{16}$ (PDF#36-1693, QM: indexed, I), anthracene $C_{14}H_{10}$ (PDF#39-1848, QM: star, S), and acenaphthylene $C_{12}H_8$ (PDF#30-1503, QM: star, S). The molecular structures of those phases are presented in Figure 4.

The interpretation results of the XRD pattern of CNPs-C are in agreement with the results reported by Beck et al.[30, 39], who performed arc discharge in toluene using carbon electrodes. Beck et al. confirmed the molecular characteristics of the product by gas chromatography-mass spectrometer (GC-MS). They found the products upon electric discharge of carbon electrodes in toluene are a polycyclic aromatic hydrocarbon and fullerene C_{60}, including acenaphthylene $C_{12}H_8$ anthracene $C_{14}H_{10}$, and hydroanthracene[30]. However, the data such as diffraction, FTIR, and Raman spectra were not shown up in their reports[30, 39].

The reaction taking place under this condition is gradual dehydrogenation, carbonization of toluene, resulting in fullerene C_{60} as the final product, dissolved in the remaining liquid medium of toluene. Figures 4(a-d) present the molecular structures of the polycyclic aromatic hydrocarbon detected by XRD, such as anthracene ($C_{14}H_{10}$), acenaphthylene ($C_{12}H_8$), 1,4,5,8,9,10-Hexahydroanthracene ($C_{14}H_{16}$), and fullerene $C_{60,}$ in which all molecules are consisting of hexagonal and pentagonal carbon rings. As illustrated in Figure 4, these hydrocarbon fragments might be as precursors for the C_{60} fullerene growth, because they possibly form the structure of the pentagonal isolated by hexagonal rings as a basic structure of fullerenes.

On the other hand, CNPs-B has the peak C(002) with highest intensity among other CNPs; thus, its crystallite size of C(002) is the largest. During arc discharge, the spot where CNPs collected between the electrodes had the highest temperature, leading for better graphitic structure formation, hence giving the peak C(002) has the highest intensity. Table 2 presents the crystallite size of the crystalline phase of CNPs. The crystallite size of CNPs from each distinguished peak is estimated around 10 nm for carbon peaks, around 20 – 30 nm for peaks of fullerene and its derivatives, and the larger size for DLC. Therefore, the estimated crystallite sizes suggest that CNPs produced are nanocrystalline carbon particles.

TEM characterization was carried out to identify the structure of the CNPs collected at different spots. Based on FTIR and the XRD data, CNPs-A have been analyzed as hydrogenated amorphous carbon or DLC. Meanwhile, because CNPs-B and -D' have a similar pattern FTIR and XRD patterns; they need to be analyzed further. Therefore, TEM analysis was performed for CNPs-B and CNPs-D', resulting in the structural images and the representative histograms, as shown in Figure 5. TEM imaging also was conducted for CNPs-C to distinguish the structural differences to CNPS-B and CNPs-D'.

The TEM images for CNPs-B, -C, and -D are shown in Figures 5(a-d, e-h, and i-l), respectively. Figure 5 show a regular morphology of narrow graphene flakes assigned by yellow arrows in Figure 5(a) and spherical carbon particles (see Figures 5(b-c)) with a non-neatly graphitic structure. The imaging analysis confirms that the graphite structures has a defect, as predicted by the feature of C(002) peak in the XRD analysis. Figures 5(e-h) and 5(i-l) show that both CNPs-B and CNPs-D' have a spherical shape with nearly same diameter. The particle size distribution of CNPs-B is approximately 26 – 44 nm, with the majority found to be ~30 nm.

Meanwhile, the image of CNPs-C revealed that the carbon particles are stacked on top of one another, and no graphitic layer was observable. Moreover, as shown in Figures 5(e-h), TEM images shows fullerene-related

structures, as predicted by FTIR and XRD analysis; some example of the fullerene rings were assigned by red arrows in Figure 5(g). Particle size distribution for the synthesized CNPs-C and CNPs-D' are both approximately 16 – 40 nm, with the majority found to be ~25 nm. The data indicated that CNPs created by arc discharge in toluene have almost the same particle size regardless of the location they are formed in. Moreover, CNPs-D' have a slightly neatly arranged graphitic structure shown as curly graphitic layers, which look significantly different from the other CNPs.

Based on the XRD data, CNPs-B and D' has a similar diffraction pattern and FTIR spectra, indicate that they have a similar crystallinity and structure. In TEM analysis of Figures 5(a-c) and 5(i-k), both CNPs-B and -D also have similar features; therefore, further characterizations are required, e.g., using Raman spectroscopy and SEM-EDX analysis to confirm the detailed structure, morphology, and content of the element, respectively.

Figure 6(a-b) shows the Raman spectra of CNPs-B and CNPs-D'. Both Raman profiles show D- and G-bands located at around 1350 and 1580 cm^{-1}, which generally represents to C−C and C=C bonding, respectively. Thus, the D- and G-bands generally represent the disorder and orderliness of graphitic structure, respectively. The G-band versus D-band ratio of Raman intensity describes the ordered or disordered state of graphite[40]. A disordered graphite state shows the domination of the structure of the sp^3 bond, as evidenced by the presence of D-band. The sp^3 bond interprets as a defect in the hexagonal sp^2 of carbon structure[41]. Therefore, the I_D/I_G ratio represents the magnitude of the defect in the hexagonal carbon structure, as shown in Table 3.

Both Raman spectra in Figure 6 show that the value of G-band intensity is higher than D-band, which indicates that the sp^2 bond was more dominant than the sp^3 bond in the structure of the CNPs. The higher G-band intensity of CNPs-B confirms that CNPs-B has better graphitization than CNPs-D'. This phenomenon was also in agreement with the XRD analysis showing that CNPs-B has the most intense peak of C(002). However, the presence of D-band indicates that the graphitic structure of CNPs-B also has defects. Considering the presence of D-band, the I_D/I_G ratios were calculated, resulting in a lower I_D/I_G ratio for CNPs-B than that of ratio for CNPs-D, as shown in Table 3.

In the Raman analysis, the shifting of the D- or G-bands also relates to the molecular structures. The G-

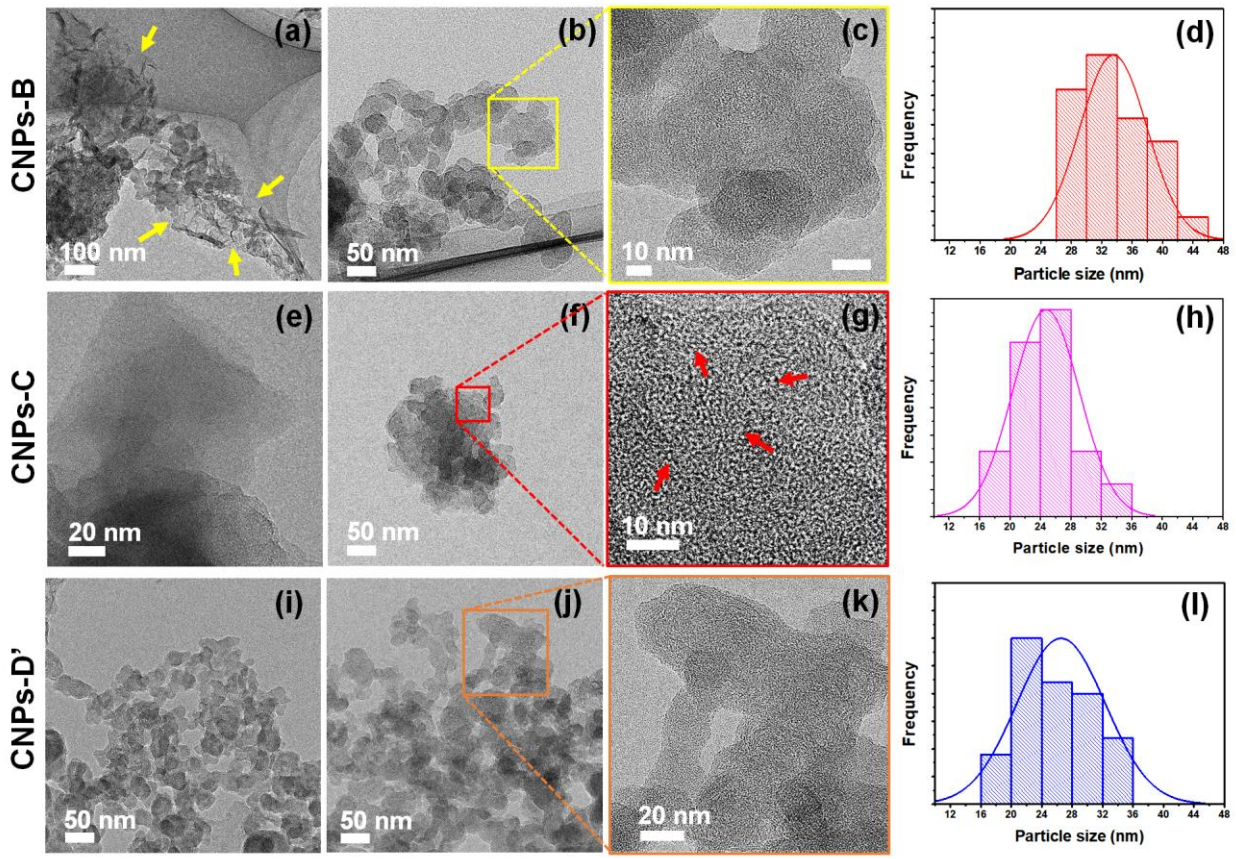

Fig 5: TEM imaging and particle size histogram of the synthesized CNPs produced via submerged arc discharge in toluene—CNPs B (a - d); CNPs C (e - h) and CNPs D' (i - l). The yellow and red arrows represent to some examples of the graphene flakes, and the fullerenes or its fragments, respectively.

band in Raman spectra, as shown in Figure 6, noticeably shifted as 14 cm^{-1} from 1579 cm^{-1} in CNPs-B to 1593 cm^{-1} in CNPs-D'. This upshift in frequencies of G-band correlated to the doping caused by other elements[42]. Simply, this shift can be understood as follows: G-band represents to C=C; so when another atom with high energy attacked, the double bonds in C=C open and change to C−C. It is well known that π-bond in C=C has lower binding energy than σ-bond in C−C, resulting in the shifting of the G-band to a higher frequency. In this case, as discussed earlier, this possibly indicates that CNPs-D' has more defects by hydrogen atoms coming from the decomposed toluene during arc discharge.

Meanwhile, CNPs-B has fewer defects because produced in the plasma zone (between the carbon electrodes), where the local temperature is very high to several thousand Kelvin[29], which induced the graphitization. Therefore, CNPs-B has more graphite layers compared to CNPs-D' which is in line with the shifting of Raman frequencies of D-, G-, and 2D-bands in Figure 6(a-b). The D- and 2D-bands undergo redshift from 1349 to 1347 cm^{-1} and 2692 to 2642 cm^{-1}, respectively; however, the G-band is blue shifted. The shifting indicates the reduction of the number of layers of graphene[43].

Moreover, the presence of the intense 2D-band observed at 2690 cm^{-1}, together with D-band, indicates structural defects in the graphite layers, which may represent another form of carbon. Theoretically, the increasing 2D band and the increasing ratio of I_{2D}/I_G associate with the number of graphene layers[44, 45]. The I_{2D}/I_G of CNPs-B is calculated as 0.711, indicative of more layers of graphene, including carbon nanocapsule or carbon onions[41]. This suggestion is in line with the TEM imaging shown in Figure 5(a-c).

CNPs-D' was CNPs collected at the bottom of the beaker glass after the arc discharge process was terminated. CNPs-D' may contain the large particles making it more likely to settle. Although, based on the XRD and FTIR data, it concludes that CNPs-D' has graphitic layers with limited defect due to no significantly observable C-H stretching in the wavenumber 2800-3000 cm^{-1} in its FTIR spectrum (see Figure 2), the structure of the particles has not been ensured yet. Using Raman spectroscopy, the carbon structure of CNPs-D' is different from CNPs-B.

According to Raman spectra of CNPs-D' as shown in Figure 6(b), a broader D-band indicates the existence of defects or disordered graphite. The increasing D-band could correspond to the higher content of sp^3 hybridized carbon atoms. The sp^2 hybridized carbon atoms (C=C bonds) mostly have been defected. The intensity of D-band of CNPs-D' is higher than that of CNPs-B, resulting in higher I_D/I_G ratio as indicative of the presence of more defects. More defects in CNPs-D' suggests the proposed structure of glass-like carbon, which in line with Raman data of glassy carbon published by the pioneering works[16, 46]. In general, glass-like carbon (GC) has a partially graphitized structure, which is a very stable form of carbon. GC has a turbostratic structure[17], which potentially made by chemical reaction of organic compounds[16]. However, GC is known as a non-amorphous carbon because it still consists of the crystalline phase eventhough in micro or nano size. As discussed earlier, the crystalline plane of C(002) CNPs-D' around 26° revealed in low intensity with the estimated crystallite size in nanometer.

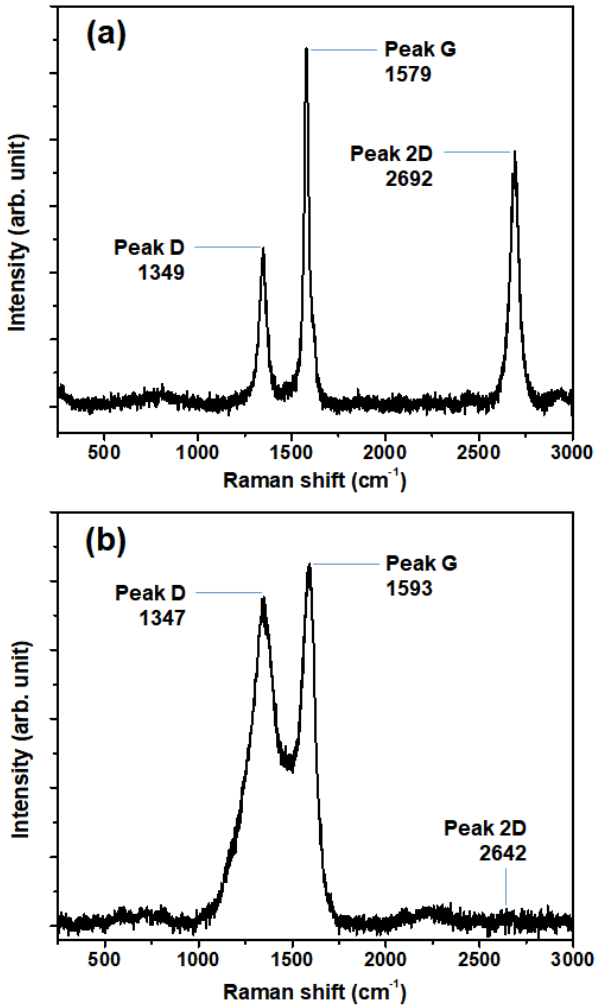

Fig 6: Raman spectra of the synthesized CNPs-B (a) and CNPs D' (b).

Table 3. I_D/I_G ratio of CNPs

Carbon nanoparticles (CNPs)	I_D/I_G	I_{2D}/I_G
CNPs-B	0.444	0.711
CNPs-D'	0.909	0.045

To confirm the morphology and the content of the dominant element, CNPs-B and D' were then analyzed by SEM-EDS. As shown in Figures 7 and 8, the morphological particles of both CNPs-B and CNPs-D' shows as spherical forms, which are in line with TEM

analysis (see Figure 5). Moreover, the element composition analysis confirms that carbon is the dominant element with an amount of more than 90 atomic percent (%At). Another element detected is oxygen; however, in very less amount < 1 At%. As described in FTIR analysis, the oxygen content is possibly coming from the hydroxyl (O−H) group of H_2O, which physically adsorbed onto the material surface.

As a final discussion, a comprehensive comparison of the data obtained to the pioneering works is required. In general, it is noticeable that the CNPs produced via arc discharge in liquid medium (such as water or organic compounds) using catalysts provide neat graphite layers. Sano et al. reported the formation of carbon onions and nanotubes by an arc in de-ionized water and liquid N_2 using carbon electrodes with 30 A electrical DC (no gas added)[47-49]. Similar works, reported by Lange et al. who used 40 A DC in submerged arc discharge in water without additional gases using both carbon electrodes, or catalyst filled carbon electrodes pairing with a carbon-only electrode. The results of carbon onion can be obtained without metal catalyst, while the metal-filled multiwalled carbon nanotubes (MWNTs) were obtained when using catalyst[27]. Similar to Lange et al., Biro et al. produced three main constituents such as agglomerates MWNTs, bucky onion type structures, soot, and graphitic particles, by applying higher AC, i.e., 85 A underwater arc using carbon electrodes with no gas added[50]. Although, no gases added, arc discharge underwater typically produces gas bubbles during processing, supplied by electrolytic decomposition of water, which then reacted with the C atomic vapors at the gas-liquid interface giving CO and H_2 gases[50, 51].

In a non-aqueous medium, Sano et al. also reported the carbonaceous structures formed at the cathode tip by the arc in benzene (with N_2 gas supply) using 50 A with graphite electrodes. The use of N_2 gas aimed to avoid the explosion of the evaporated benzene. The various structures produced are agglomerated multi-shelled CNPs, graphite balls, and highly curled graphite[52]. Continuing what was done by Sano et al., in the same electrical DC of 50 A using graphite electrodes (with N_2 gas), Muthakarn et al. analyzed the similar of various carbon structure produced by an arc in organic compounds (e.g., alcohol, alkane, benzene, toluene, and ethylbenzene), such as multi-shelled nanoparticles, graphite, amorphous, disordered carbon, and MWNTs (except in benzene)[29].

Okada et al. confirmed the nanocarbon structures formed by arc discharge plasma in toluene with and without catalyst using 20 A DC (no additional gases added). Spheroidal shaped nanocarbons are observable when using graphite electrodes without using metal catalysts. Raman spectra and TEM imaging reveal a similar feature to our works. In the case that nickel catalyst was used as electrodes, the structure of the nanocarbon consisted of graphite sheets was detectable[26].

In brief, lower electrical DC provides spherical nanocarbon particles. In contrast, the higher ones can produce the carbon particles with neater graphitic structures in higher aspect ratio, such MWNTs accompanied by amorphous or disordered carbon. Comparing to the pioneering works discussed, our present study described the differences structures of carbon particles produced by an arc in low DC of 30 A, which provide similar results to the pioneering works using 20 A.

According to the results have been discussed herein, arc discharge using carbon electrodes in toluene produced various products of CNPs in a graphitic structure, which defected by hydrogen atoms. The benefit of the use of pure toluene with no gases in this experiment is to avoid the formation of oxygen-containing gases. In the hot plasma zone, the oxygen-containing gas possibly evaporates and ionizes and then involves in CNPs formation resulting in more defect sites by oxygen atoms giving amorphous carbon. Meanwhile, as presented in this study, when toluene was used as medium in liquid arc discharge, only hydrogen plasma was supposedly involved, resulted in selective etching of carbon facets, and terminated as sp^3 −C−H species[53].

Overall, the less defected CNPs were confirmed for CNPs produced between the carbon electrodes, while the

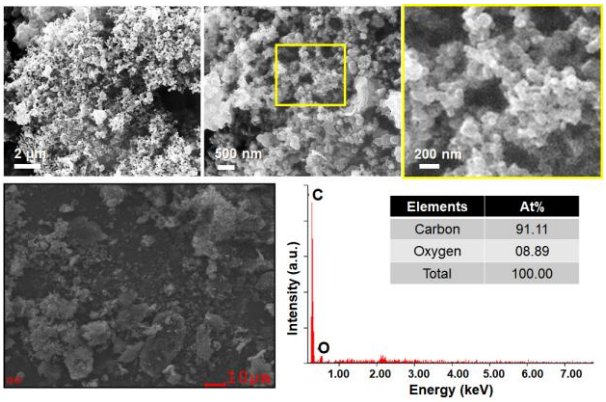

Fig 7: SEM-EDS of CNPs-B, the element composition was shown in table.

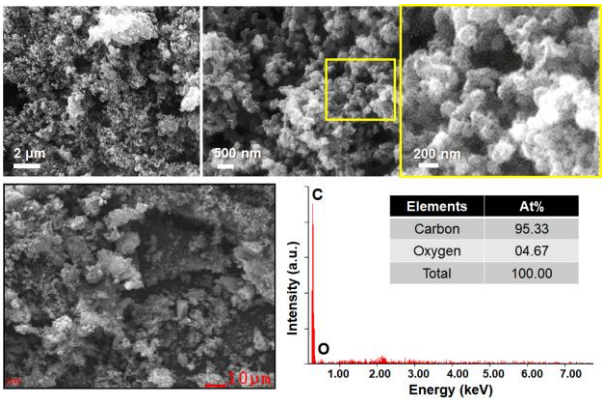

Fig 8: EM-EDS of CNPs-D', the element composition was shown in table.

more defected CNPs were found for CNPs settled down on the bottom of the beaker glass. Moreover, the most different structure was also obtained for CNPs simultaneously dissolved in arc discharge liquid medium of toluene, which is possibly as fullerenes and its derivatives of the organic molecular fragments.

4. Conclusions

The study of the structural characteristics of CNPs produced in a submerged arc discharge using a liquid medium of toluene revealed differences between CNPs collected from different spots such as between those collected in the liquid medium, between electrodes, and at the bottom of the chamber glass. The dominant structure was a graphitic arrangement with structural defects, which were confirmed by FTIR, XRD, and D- and G-bands in Raman spectra. According to the XRD data, the most intense graphitic structures belonged to the CNPs collected between the electrodes. CNPs collected from the liquid medium of toluene mostly contained fullerene and polycyclic aromatic hydrocarbon. Meanwhile, CNPs collected from the electrode handle and the bottom of the chamber consisted of DLC and glassy carbon bulk, respectively.

Acknowledgments

This work was financially supported by Minister of Research, Technology and Higher Education, the Republic of Indonesia in grant under Project No. 719/UN27.21/PN/2019 and 452/UN27.21/PN/2020.

References

1) X. Zhang, B.R.S. Rajaraman, H. Liu, and S. Ramakrishna, "Graphene's potential in materials science and engineering," *RSC Adv.,* **4** (*55*) 28987-29011 (2014). doi:10.1039/c4ra02817a.
2) D.M. Guldi, and V. Sgobba, "Carbon nanostructures for solar energy conversion schemes," *Chem. Commun.,* **47** (*2*) 606-610 (2011). doi:10.1039/c0cc02411b.
3) C.X. Guo, H.B. Yang, Z.M. Sheng, Z.S. Lu, Q.L. Song, and C.M. Li, "Layered Graphene/Quantum Dots for Photovoltaic Devices," *Angew. Chem. Int. Ed.,* **49** (*17*) 3014-3017 (2010). doi:10.1002/anie.200906291.
4) Y. Zhang, L.F. Duan, Y. Zhang, J. Wang, H. Geng, and Q. Zhang, "Advances in Conceptual Electronic Nanodevices based on 0D and 1D Nanomaterials," *Nano-Micro Lett.,* **6** (*1*) 1-19 (2014). doi:10.1007/bf03353763.
5) S. Ramanathan, S.C.B. Gopinath, M.K. Md. Arshad, and P. Poopalan, "Multidimensional (0D-3D) nanostructures for lung cancer biomarker analysis: Comprehensive assessment on current diagnostics," *Biosens. Bioelectron.,* **141** 111434 (2019). doi:10.1016/j.bios.2019.111434.
6) J. Yao, P. Li, L. Li, and M. Yang, "Biochemistry and biomedicine of quantum dots: from biodetection to bioimaging, drug discovery, diagnostics, and therapy," *Acta Biomater.,* **74** 36-55 (2018). doi:10.1016/j.actbio.2018.05.004.
7) S. Zhu, Y. Song, X. Zhao, J. Shao, J. Zhang, and B. Yang, "The photoluminescence mechanism in carbon dots (graphene quantum dots, carbon nanodots, and polymer dots): current state and future perspective," *Nano Res.,* **8** (*2*) 355-381 (2015). doi:10.1007/s12274-014-0644-3.
8) X. Sun, J. He, Y. Meng, L. Zhang, S. Zhang, X. Ma, S. Dey, J. Zhao, and Y. Lei, "Microwave-assisted ultrafast and facile synthesis of fluorescent carbon nanoparticles from a single precursor: preparation, characterization and their application for the highly selective detection of explosive picric acid," *J. Mater. Chem. A.,* **4** (*11*) 4161-4171 (2016). doi:10.1039/c5ta10027e.
9) G. Zhu, T. Chen, Y. Hu, L. Ma, R. Chen, H. Lv, Y. Wang, J. Liang, X. Li, and C. Yan, "Recycling PM2. 5 carbon nanoparticles generated by diesel vehicles for supercapacitors and oxygen reduction reaction," *Nano Energy,* **33** 229-237 (2017). doi:10.1016/j.nanoen.2017.01.038.
10) M. Ajmal, U. Yunus, A. Matin, and N.U. Haq, "Synthesis, characterization and in vitro evaluation of methotrexate conjugated fluorescent carbon nanoparticles as drug delivery system for human lung cancer targeting," *J. Photochem. Photobiol. B, Biol.,* **153** 111-120 (2015). doi:10.1016/j.jphotobiol.2015.09.006.
11) N. De Greef, L. Zhang, A. Magrez, L. Forró, J.-P. Locquet, I. Verpoest, and J.W. Seo, "Direct growth of carbon nanotubes on carbon fibers: Effect of the CVD parameters on the degradation of mechanical properties of carbon fibers," *Diam. Relat. Mater.,* **51** 39-48 (2015). doi:10.1016/j.diamond.2014.11.002.
12) J. Zhou, C. Booker, R. Li, X. Zhou, T.-K. Sham, X. Sun, and Z. Ding, "An electrochemical avenue to blue luminescent nanocrystals from multiwalled carbon nanotubes (MWCNTs)," *J. Am. Chem. Soc.,* **129** (*4*) 744-745 (2007). doi:10.1021/ja0669070.
13) D. Reyes-Contreras, M. Camacho-López, M.A. Camacho-López, S. Camacho-López, R.I. Rodríguez-Beltrán, and M. Mayorga-Rojas, "Influence of the per pulse laser fluence on the optical properties of carbon nanoparticles synthesized by laser ablation of solids in liquids," *Opt. Laser Technol.,* **74** 48-52 (2015). doi:10.1016/j.optlastec.2015.05.010.
14) H. Naragino, M. Egiza, A. Tominaga, K. Murasawa, H. Gonda, M. Sakurai, and T. Yoshitake, "Fabrication of ultrananocrystalline diamond/nonhydrogenated amorphous carbon composite films for hard coating by coaxial arc

plasma deposition," *EVERGREEN Joint Journal of Novel Carbon Resource Sciences & Green Asia Strategy,* **3** 1 (2016). doi:10.5109/1657379.

15) M.M. Sahihazar, M. Nouri, M. Rahmani, M.T. Ahmadi, and H. Kasani, "Fabrication of carbon nanoparticle strand under pulsed arc discharge," *Plasmonics,* **13** (*6*) 2377-2386 (2018). doi:10.1007/s11468-018-0764-9.
16) M.I. Nathan, J.E.S. Jr., and K.N. Tu, "Raman spectra of glassy carbon," *J. Appl. Phys.,* **45** (*5*) 2370-2370 (1974). doi:10.1063/1.1663599.
17) M. Hassler, "3 - Other commonly used biomedical coatings: pyrolytic carbon coatings. In *Coatings for Biomedical Applications*," Woodhead Publishing, 2012. http://www.sciencedirect.com/science/article/pii/B9781845695682500035.
18) C. Casiraghi, J. Robertson, and A.C. Ferrari, "Diamond-like carbon for data and beer storage," *Mater. Today.,* **10** (*1*) 44-53 (2007). doi:10.1016/S1369-7021(06)71791-6.
19) R.K. Roy, B. Deb, B. Bhattacharjee, and A.K. Pal, "Synthesis of diamond-like carbon film by novel electrodeposition route," *Thin Solid Films,* **422** (*1*) 92-97 (2002). doi:10.1016/S0040-6090(02)00976-8.
20) E. Liu, L. Li, B. Blanpain, and J.P. Celis, "Residual stresses of diamond and diamondlike carbon films," *J. Appl. Phys.,* **98** (*7*) 073515 (2005). doi:10.1063/1.2071451.
21) H. Pang, X. Wang, G. Zhang, H. Chen, G. Lv, and S. Yang, "Characterization of diamond-like carbon films by SEM, XRD and Raman spectroscopy," *Appl. Surf. Sci.,* **256** (*21*) 6403-6407 (2010). doi:10.1016/j.apsusc.2010.04.025.
22) A. Ashkarran, "Metal and metal oxide nanostructures prepared by electrical arc discharge method in liquids," *J. Clust. Sci.,* **22** (*2*) 233 (2011). doi:10.1007/s10876-011-0376-4.
23) R. Sharma, A.K. Sharma, and V. Sharma, "Synthesis of carbon nanotubes by arc-discharge and chemical vapor deposition method with analysis of its morphology, dispersion and functionalization characteristics," *Cogent Eng.,* **2** (*1*) 1094017 (2015). doi:10.1007/s10876-011-0376-4.
24) N. Sano, H. Wang, M. Chhowalla, I. Alexandrou, and G. Amaratunga, "Nanotechnology: Synthesis of carbon'onions' in water," *Nature,* **414** (*6863*) 506 (2001). doi:10.1038/35107141.
25) Y.L. Hsin, K.C. Hwang, F.-R. Chen, and J.-J. Kai, "Production and in-situ Metal Filling of Carbon Nanotubes in Water," *Adv. Mater.,* **13** (*11*) 830-833 (2001). doi:10.1002/1521-4095(200106)13:11<830::Aid-adma830>3.0.Co;2-4.
26) T. Okada, T. Kaneko, and R. Hatakeyama, "Conversion of toluene into carbon nanotubes using arc discharge plasmas in solution," *Thin Solid Films,* **515** (*9*) 4262-4265 (2007). doi:10.1016/j.tsf.2006.02.067.
27) H. Lange, M. Sioda, A. Huczko, Y.Q. Zhu, H.W. Kroto, and D.R.M. Walton, "Nanocarbon production by arc discharge in water," *Carbon,* **41** (*8*) 1617-1623 (2003). doi:10.1016/S0008-6223(03)00111-8.
28) U. Kumar, S. Sikarwar, R.K. Sonker, and B. Yadav, "Carbon nanotube: synthesis and application in solar cell," *J. Inorg. Organomet. Polym. Mater.,* **26** (*6*) 1231-1242 (2016). doi:10.1007/s10904-016-0401-z.
29) P. Muthakarn, N. Sano, T. Charinpanitkul, W. Tanthapanichakoon, and T. Kanki, "Characteristics of Carbon Nanoparticles Synthesized by a Submerged Arc in Alcohols, Alkanes, and Aromatics," *J. Phys. Chem. B.,* **110** (*37*) 18299-18306 (2006). doi:10.1021/jp063443j.
30) M.T. Beck, Z. Dinya, S. Kéki, and L. Papp, "Formation of C60 and polycyclic aromatic hydrocarbons upon electric discharges in liquid toluene," *Tetrahedron,* **49** (*1*) 285-290 (1993).
31) P.-X. Hou, C. Liu, and H.-M. Cheng, "Purification of carbon nanotubes," *Carbon,* **46** (*15*) 2003-2025 (2008). doi:10.1016/j.carbon.2008.09.009.
32) F.T.L. Muniz, M.A.R. Miranda, C. Morilla dos Santos, and J.M. Sasaki, "The Scherrer equation and the dynamical theory of X-ray diffraction," *Acta Crystallographica Section A: Foundations and Advances,* **72** (*3*) 385-390 (2016). doi:10.1107/S205327331600365X.
33) V. Ţucureanu, A. Matei, and A.M. Avram, "FTIR spectroscopy for carbon family study," *Crit. Rev. Anal. Chem.,* **46** (*6*) 502-520 (2016). doi:10.1080/10408347.2016.1157013.
34) Y. Nakata, "Algorithms used for data processing in FTIR," *FTIR Talk Letter,* **10** 4 (2008).
35) T.E. Saraswati, I. Retnosari, I.N. Hayati, A. Amalia, and S. Hastuti, "The Influence of Ammonia Addition on the Surface Characteristics of Fe3O4/Carbon Nanoparticles in Submerged Arc Discharge," *Recent Pat. Mater. Sci.,* **11** (*2*) 71-82 (2018). doi:10.2174/1874464812666181128102742.
36) J. Coates, "Interpretation of infrared spectra, a practical approach. In *Encyclopedia of Analytical Chemistry*," Wiley Online Library, 2006. https://onlinelibrary.wiley.com/doi/abs/10.1002/9780470027318.a5606.
37) B.C. Smith, "Distinguishing structural isomers: mono-and disubstituted benzene rings," *Spectroscopy,* **31** (*5*) 36-39 (2016).
38) Z.Q. Li, C.J. Lu, Z.P. Xia, Y. Zhou, and Z. Luo, "X-ray diffraction patterns of graphite and turbostratic carbon," *Carbon,* **45** (*8*) 1686-1695 (2007). doi:10.1016/j.carbon.2007.03.038.
39) M.T. Beck, Z. Dinya, and S. Kéki, "Formation of polycyclic aromatic compounds upon electric discharges in liquid toluene," *Tetrahedron,* **48** (*23*) 4919-4928 (1992). doi:10.1016/S0040-4020(01)81584-2.

40) G.G. Hoffmann, G. de With, and J. Loos In *Micro‐Raman and Tip‐Enhanced Raman Spectroscopy of Carbon Allotropes*, Macromolecular symposia, Wiley Online Library: 2008; pp 1-11.
41) M. Couzi, J.-L. Bruneel, D. Talaga, and L. Bokobza, "A multi wavelength Raman scattering study of defective graphitic carbon materials: The first order Raman spectra revisited," *Carbon,* **107** 388-394 (2016). doi:10.1016/j.carbon.2016.06.017.
42) J. Hong, M.K. Park, E.J. Lee, D. Lee, D.S. Hwang, and S. Ryu, "Origin of New Broad Raman D and G Peaks in Annealed Graphene," *Sci. Rep.,* **3** (*1*) 2700 (2013). doi:10.1038/srep02700.
43) X.X. Yang, J.W. Li, Z.F. Zhou, Y. Wang, L.W. Yang, W.T. Zheng, and C.Q. Sun, "Raman spectroscopic determination of the length, strength, compressibility, Debye temperature, elasticity, and force constant of the C–C bond in graphene," *Nanoscale,* **4** (*2*) 502-510 (2012). doi:10.1039/c1nr11280e.
44) L.M. Malard, M.A. Pimenta, G. Dresselhaus, and M.S. Dresselhaus, "Raman spectroscopy in graphene," *Phys. Rep.,* **473** (*5*) 51-87 (2009). doi:10.1016/j.physrep.2009.02.003.
45) T.-o. Terasawa, and K. Saiki, "Growth of graphene on Cu by plasma enhanced chemical vapor deposition," *Carbon,* **50** (*3*) 869-874 (2012). doi:10.1016/j.carbon.2011.09.047.
46) L.A. Pesin, "Review Structure and properties of glass-like carbon," *J. Mater. Sci.,* **37** (*1*) 1-28 (2002). doi:10.1023/A:1013100920130.
47) N. Sano, M. Naito, M. Chhowalla, T. Kikuchi, S. Matsuda, K. Iimura, H. Wang, T. Kanki, and G.A.J. Amaratunga, "Pressure effects on nanotubes formation using the submerged arc in water method," *Chem. Phys. Lett.,* **378** (*1*) 29-34 (2003). doi:10.1016/S0009-2614(03)01246-6.
48) N. Sano, H. Wang, I. Alexandrou, M. Chhowalla, K.B.K. Teo, G.A.J. Amaratunga, and K. Iimura, "Properties of carbon onions produced by an arc discharge in water," *J. Appl. Phys.,* **92** (*5*) 2783-2788 (2002). doi:10.1063/1.1498884.
49) N. Sano, H. Wang, M. Chhowalla, I. Alexandrou, and G.A.J. Amaratunga, "Synthesis of carbon'onions' in water," *Nature,* **414** (*6863*) 506 (2001). doi:10.1038/35107141.
50) L.P. Biró, Z.E. Horváth, L. Szalmás, K. Kertész, F. Wéber, G. Juhász, G. Radnóczi, and J. Gyulai, "Continuous carbon nanotube production in underwater AC electric arc," *Chem. Phys. Lett.,* **372** (*3*) 399-402 (2003). doi:10.1016/S0009-2614(03)00417-2.
51) N. Sano, H. Wang, I. Alexandrou, M. Chhowalla, K. Teo, G. Amaratunga, and K. Iimura, "Properties of carbon onions produced by an arc discharge in water," *J. Appl. Phys.,* **92** (*5*) 2783-2788 (2002). doi:10.1063/1.1498884.
52) N. Sano, "Formation of multi-shelled carbon nanoparticles by arc discharge in liquid benzene," *Mater. Chem. Phys.,* **88** (*2*) 235-238 (2004). doi:10.1016/j.matchemphys.2004.07.018.
53) Z. Shpilman, I. Gouzman, E. Grossman, R. Akhvlediani, and A. Hoffman, "Hydrogen plasma and atomic oxygen treatments of diamond: Chemical versus morphological effects," *Appl. Phys. Lett.,* **92** (*23*) 234103 (2008). doi:10.1063/1.2939561.